Raman Storage of Quasideterministic Single Photons Generated by Rydberg Collective Excitations in a Low-Noise Quantum Memory

L. Heller,[1,*,‡] J. Lowinski,[1,†,‡] K. Theophilo,[1] A. Padrón-Brito,[1] and H. de Riedmatten[1,2]

[1] *ICFO—Institut de Ciencies Fotoniques, The Barcelona Institute of Science and Technology, Barcelona 08860 Castelldefels, Spain*

[2] *ICREA—Institució Catalana de Recerca i Estudis Avançats, Barcelona 08015, Spain*

(Received 19 November 2021; revised 14 June 2022; accepted 17 June 2022; published 12 August 2022)

We demonstrate the storage and retrieval of an on-demand single photon generated by a collective Rydberg excitation in a low-noise Raman quantum memory located in a different cold atomic ensemble. We generate single photons on demand by exciting a cold cloud of rubidium atoms off resonantly to a Rydberg state, with a generation probability up to 15% per trial. We then show that the single photons can be stored and retrieved with a storage-and-retrieval efficiency of 21% and a low noise floor in the Raman quantum memory. This leads to a signal-to-noise ratio ranging from 11 to 26 for the retrieved single photon, depending on the input-photon-generation probability, which allows us to observe significant antibunching. We also evaluate the performance of the Raman memory as a built-in unbalanced temporal beam splitter, tunable by varying the write-in control-pulse intensity. In addition, we demonstrate that the Raman memory can be used to control the single-photon wave shape. These results are a step forward in the implementation of efficient quantum repeater links using single-photon sources.

DOI: 10.1103/PhysRevApplied.18.024036

I. INTRODUCTION

The development of quantum networks [1] is one of the most active branches of quantum technologies. A fundamental step toward long-distance quantum communications would be the realization of efficient quantum repeaters [2–4] that would allow the distribution of entanglement over distances longer than is achievable with direct photon transmission. Near-term quantum repeaters are based on heralded entanglement between remote quantum memories (QMs) that form an elementary repeater link and on entanglement swapping between the elementary links to extend the entanglement distance. Various platforms have been considered as quantum memories for quantum repeaters, including single atoms [5,6] or ions [7–10], cold atomic clouds [11–18] and solid-state systems such as color centers in diamond [19,20] or rare-earth-doped solids [21–26]. Ensemble-based approaches are promising for reaching high-rate quantum repeaters because they enable large multiplexing, which increases the rate of entanglement in elementary links proportionately to the number of stored modes [17,25,27–31].

To date, most of the early demonstrations of quantum repeater links with ensemble-based quantum memories are based on probabilistic light-matter entanglement sources, e.g., based on emissive quantum memories using spontaneous Raman scattering in atomic clouds [12–14,18,32], following the Duan, Lukin, Cirac, and Zoller (DLCZ) proposal, or by using read-write quantum memories combined with spontaneous parametric down-conversion sources [25,26]. However, these types of probabilistic sources lead to limitations due to a trade-off between the excitation probability and fidelity of the generated state. To keep the errors due to the generation of multiple pairs low and therefore the fidelity high, the generation probability must remain low. This trade-off leads to low success probability per trial (especially for multiple-link repeaters), which limits the overall high-fidelity entanglement rate [4].

A quantum repeater architecture based on the use of deterministic single photons and absorptive ensemble-based quantum memories has been proposed to overcome this limitation [33]. In this scheme, each node consists of a deterministic single-photon source and a quantum memory. The single photon is sent on a beam splitter (BS) and one output of the BS is directed toward the quantum memory while the other output is converted to telecom wavelength and sent to a central station, where

*Corresponding author. lukas.heller@icfo.eu
†Corresponding author. jan.lowinski@icfo.eu
‡These two authors contributed equally

it is mixed with the photonic mode from another distant quantum node. It has been shown that heralded single photons (generated from probabilistic sources) can be stored in quantum memories [34,35] with up to 87% storage-and-retrieval efficiency [16,36]. Hence, the main challenge of this scheme compared to schemes using probabilistic sources is to generate memory-compatible indistinguishable single photons on demand with high efficiency. In addition, the quantum memory should feature very low noise in order not to degrade the single-photon properties.

Several approaches have been demonstrated to generate on-demand single photons using single emitters such as quantum dots, single molecules, and color centers in diamond. However, most of these photons are not resonant with quantum memories and have a bandwidth much larger than that of long-lived quantum memories. While progress has been made recently to interface photons from quantum dots and molecules to atomic vapors or rare-earth-doped solids [37–40], so far high efficiency and long-lived storage of these photons has not been demonstrated. Single trapped atoms can be used to generate directly resonant and memory-compatible photons that have been interfaced with a Bose-Einstein condensate (BEC) quantum memory [41]; however, efficient photon generation in a single mode requires placing the atom in a high-finesse cavity, which represents an experimentally complex task. In recent years, several experiments have shown that ensembles of Rydberg atoms could serve as a source of on-demand narrow-band [42–45] indistinguishable single photons [46–48]. This approach has the advantage that no high-finesse cavity is required, due to the collective nature of the single-photon generation.

In this paper, we demonstrate the storage and retrieval of an on-demand single photon generated by collective Rydberg excitation on a low-noise Raman quantum memory located in a different cold atomic ensemble. We show that the single photons can be stored and retrieved with a signal-to-noise ratio (SNR) up to 26, preserving strong antibunching. We also evaluate the performance of the built-in temporal beam splitter offered by the Raman memory. In addition, we demonstrate that the Raman memory can be used to control the single-photon wave shape. These results show that single photons generated on demand by Rydberg atoms can be stored in an atomic quantum memory, which is a potentially important step toward the implementation of efficient quantum repeater links using single-photon sources.

II. EXPERIMENTAL SETUP

Our experimental setup comprises of two ensembles of cold ^{87}Rb atoms situated in the same laboratory connected via 12 m of optical-fiber cable. One of them is used to generate single photons in a quasideterministic way by exploiting the strong dipole-dipole interaction between Rydberg states (the source). Another is used to store and retrieve on demand the generated photons in an atomic Raman memory.

In the first step of the generation protocol, we excite the ensemble from its ground state $|g_s\rangle = |5S_{1/2}, F = 2\rangle$ to a Rydberg state $|r\rangle = |90S_{1/2}\rangle$ [see Fig. 1(d)] via a two-photon excitation. We send a weak coherent probe pulse Ω_p and a strong counterpropagating coupling pulse $\Omega_c \approx 6$ MHz [see Fig. 1(a)]. The $1/e^2$ beam radius is 6.5 μm for the probe and 13 μm for the coupling mode. The probe light at a wavelength of 780 nm is red detuned by -40 MHz from the transition to the excited state $|e_s\rangle = |5P_{3/2}, F = 3\rangle$. The coupling light is tuned such that the two-photon transition is resonant with the transition $|g_s\rangle \rightarrow |r\rangle$.

The number of generated Rydberg excitations is strongly limited due to the dipole blockade [49]. The blockade is a result of the strong dipole-dipole interaction between Rydberg states, which prevents a simultaneous excitation of two Rydberg atoms if they are closer than a distance called the blockade radius. Then, if the interaction region is smaller than the volume given by the blockade radius, only one atomic excitation will be created in state $|r\rangle$—this is called the fully blockaded regime. The Rydberg excitation is shared between all the atoms in the blockade region, forming a collective quantum superposition, termed a Rydberg spin wave.

With a delay of 1 ms, a second coupling pulse is sent resonantly to the $|r\rangle \rightarrow |e_s\rangle$ transition, mapping the Rydberg spin wave onto the excited state $|e_s\rangle$ and triggering the collective emission of a single photon at 780 nm. The photon is emitted in the input mode and in the forward direction due to collective atomic interference. It is then separated from the coupling light by a dichroic mirror and a band-pass filter, before being collected into a polarization-maintaining single-mode fiber. An electronic trigger is sent to the memory to signal each photon-generation attempt.

The generated photon is guided to the second atomic ensemble, the memory. The frequency of the photon is, however, not compatible with the transitions used in the memory, so it is shifted by -320 MHz with an acousto-optic modulator (AOM). As a result, the photon is now red detuned with respect to the $|g_m\rangle \rightarrow |e_m\rangle$ transition.

The Raman memory relies on coherent adiabatic absorption of the incoming single photon [50]. A storage attempt starts with sending a control write-in pulse Ω_W coupling states $|s\rangle = |5S_{1/2}, F = 1, m_F = 0\rangle$ and $|e_m\rangle = |5P_{3/2}, F = 2, m_F = +1\rangle$ off resonantly by $\delta = -52$ MHz [see Fig. 1(e)]. The $1/e^2$ beam radius is 69 μm for the photon and 180 μm for the coupling mode. Assuming that the $|g_m\rangle \rightarrow |e_m\rangle$ transition is lifetime limited, the excited-state coherence lifetime is $2\tau_{eg}$, with $\tau_{eg} = 26$ ns the excited-state population lifetime. Since the write-in pulse is in two-photon resonance with the input photon, the incoming photon field is transferred to a collective atomic spin

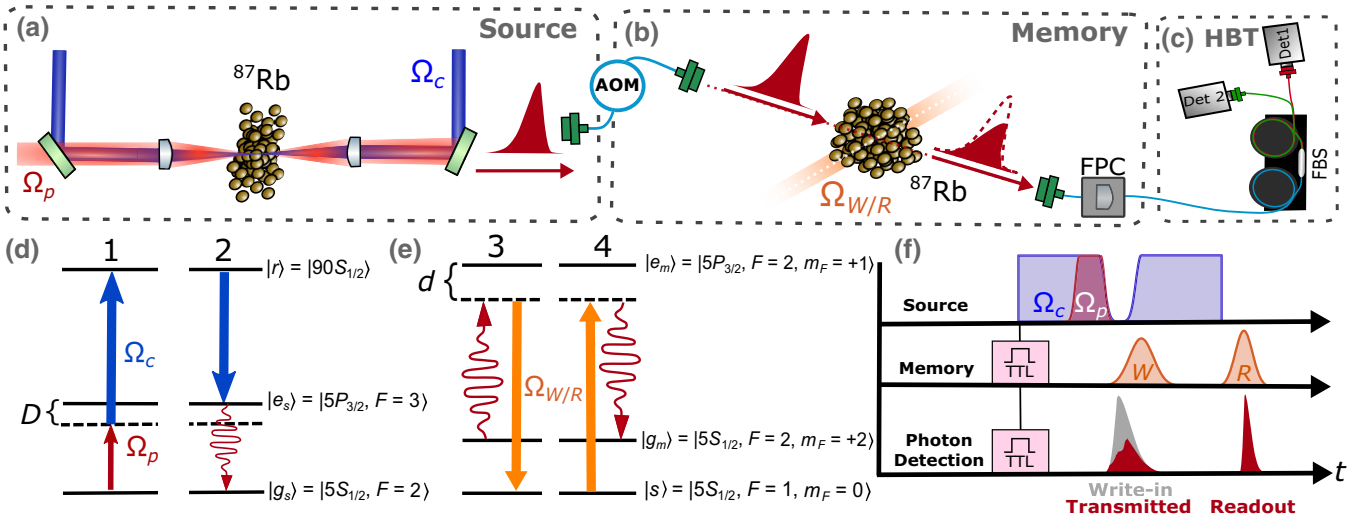

FIG. 1. A scheme of the experimental setup, the relevant atomic levels, and the experimental sequence. (a) The source. The probe (Ω_p) and the counterpropagating coupling beam (Ω_c) are tightly focused in a cold cloud of rubidium atoms to generate the input photon. (b) The memory. A write-in control-beam pulse (Ω_W) maps the incoming photon to an atomic excitation in another cold cloud of rubidium atoms. The excitation is retrieved with a readout control-beam pulse (Ω_R) and filtered with a Fabry-Perot cavity (FPC). (c) The retrieved photon is split in a fiber-based beam splitter (FBS) and detected with SNSPDs 1 and 2 performing, effectively, an HBT measurement. (d),(e) The relevant atomic levels for the photon generation (d) and for the photon storage (e) are also shown. A two-photon excitation (Ω_p and Ω_c) creates a Rydberg spin wave in $|r\rangle$ (1), which is later mapped to the first excited state $|e_s\rangle$ and decays emitting a photon (2). The emitted photon is mapped with Ω_W to a ground-state spin wave in $|s\rangle$ (3) and later retrieved with Ω_R (4). (f) The pulse sequence. The whole experiment is synchronized with TTLs sent by the source at the beginning of each generation trial.

excitation on $|s\rangle$. Careful tuning of the control write-in pulse shape, power, and timing with respect to the input photon is required to optimize the writing efficiency into the memory. Experimentally, we find that the optimum control write-in pulse closely resembles the input-photon wave shape and impinges on the cloud shortly before the photon, with $\Omega_W \approx 48$ MHz.

To retrieve the stored excitation, after a programmable delay, we send a readout pulse Ω_R. The readout pulse is in the same spatial mode as the write-in pulse with the same frequency detuning δ. Owing to the collective atomic interference, the photon is emitted in the input mode in the forward direction and collected into a single-mode fiber. The bandwidth and the shape of the output photon are governed by the temporal profile and the power of the readout pulse and can be tuned arbitrarily (see Sec. III B).

The collected photons are guided to the detection setup. Depending on the measurement, it is either a superconducting nanowire single-photon detector (SNSPD) or a Hanbury Brown–Twiss (HBT) setup comprised of a fiber-based beam splitter and two SNSPDs [see Fig. 1(c)]. We use a HBT setup to measure photon autocorrelation.

For the source to produce single photons, it is necessary for it to be in the fully blockaded regime or close to it. Moreover, the coherence time of the Rydberg transition should be much longer than the excitation-pulse duration, to keep the photon-generation probability high. In our case, this means that the ensemble needs to be cold to limit the motional dephasing. Both are achieved in the preparation stage when we first load the atoms into a magneto-optical trap (MOT), later compress them, and subsequently apply 7 ms of polarization-gradient cooling. Finally the ensemble is prepared by optical pumping to its initial ground state $|g_s\rangle = |5S_{1/2}, F = 2\rangle$. A one-dimensional dipole trap is kept on during the whole process (with a beam waist of 34 μm at an angle of 22° with respect to the probe beam and a trap depth of 0.3 mK). The whole process results in a cloud with an optical density (OD) of 6 and a temperature of 40 mK. Due to the dipole trap, the effective interaction region, given by the overlap between the probe beam and the atomic ensemble, is still larger but comparable to the approximately 13 μm of the blockade radius. The ensemble can be interrogated for 200 ms, limited by the population lifetime of the dipole trap (400 ms), before another MOT reloading cycle has to be performed. During its interrogation time, the source attempts to generate a single photon every 4 μs with generation probability $p_{\text{gen}} = 5 - 15\%$. The photon generation and the characterization of their indistinguishability are described in more detail in Ref. [48].

For the memory, the OD of the ensemble and the cloud temperature are the main parameters governing

the storage-and-retrieval efficiency and the storage time. To achieve a dense and cold ensemble, the atoms are first loaded into a MOT for 10 ms followed by 1.5 ms of polarization-gradient cooling. Later, the memory is optically pumped to its initial ground state $|g_m\rangle = |5S_{1/2}, F = 2, m_F = +2\rangle$, in the presence of a homogeneous magnetic bias field oriented along the photon mode. Optical pumping is helpful to avoid beating between spin waves at different Zeeman sublevels. The whole process provides us a cloud with an OD of 5 and a temperature of 30 mK. The OD starts dropping after 1.2 ms of interrogation time and the trapping cycle has to be repeated.

One of the main challenges of this study is the long integration times, which require good stability of both setups. This results mainly from two technical limitations. The first one is the very different trapping cycles of the source and the memory, making the overall duty cycle very low. The resulting repetition rate of the whole experiment is 5 kHz. The second one is the passive loss in the photon transmission, which affects the coincidence probability in the HBT experiment quadratically. The total transmission from the output of the source to the detection setup, in the absence of atoms in the memory, is 10(1)%, limited by the fiber coupling after the source (0.4), the frequency-shifter AOM setup (0.62), the fiber coupling after the memory (0.83), the frequency-filtering cavity setup (0.65), and miscellaneous optical and polarization-dependent losses (0.75). The transmission from the output of the source to the input of the quantum memory is 22%. The SNSPDs have a quantum efficiency of approximately 85% and 3 Hz of dark counts.

The limiting factor for the quality of the single photon retrieved from the quantum memory is the introduced technical noise, which affects its SNR. The main source of noise is the leakage of the memory control pulses that couple to the photon mode. An angle of 3° between the photon mode and the coupling beam minimizes the spatial overlap and noise introduced by directional forward scattering. The noise is further removed with a home-built narrow-band Fabry-Perot filter cavity of 43.4-dB suppression (at the control-pulse frequency). The remaining noise is composed of light leaking through the filter, inelastically scattered control light at the photon frequency, and the dark counts of the detectors.

III. RESULTS

In this section, we study the single-photon properties of the source photons, which, further on, are used as the memory input photon. Second, we discuss the performance of the memory, commenting on its tunability.

A. Photon generation

The HBT setup is used to characterize the photons generated by the source. The photon arrival times at each SNSPD are recorded together with trigger times for each experimental trial. We compute the second-order autocorrelation function as

$$g^{(2)}(k) = \frac{c_{1,2}(k)}{p_1 p_2}, \tag{1}$$

where p_1 (p_2) is the probability of detection per trial with SNSPD 1 (2) and $c_{1,2}(k)$ is the probability of a coincidence between detections separated by k trials ($k = 0$ means that detections are taken within the same trial). All the probabilities are calculated within a detection time window at fixed delay after each trial trigger. We choose a 300-ns detection window, which includes more than 95% of the photon. For perfect single photons, $g^{(2)}(0) = 0$. In practice, background noise or multiphoton components increase the $g^{(2)}(0)$. The emitted light remains nonclassical for $g^{(2)}(0) < 1$ and $g^{(2)}(0) = 0.5$ marks the limit between single- and multiphoton states.

In our source, we can change the emitted photon $g^{(2)}(0)$ within a range of 0.16 to 1 by varying the mean probe photon number (see Fig. 2). For a smaller probe photon number, the increase of $g^{(2)}(0)$ is accompanied by an increase of the photon-generation probability p_{gen}, which is defined as $p_{\text{gen}} = (p_1 + p_2)/\alpha$, where $\alpha = 0.21$ is the combined transmission and detection efficiency (of the source only—in this characterization, we detect photons right after the source). However, for a larger probe photon number, p_{gen} decreases in accordance with the Rabi cycle. Yet, this is not accompanied by the $g^{(2)}(0)$, which continues to grow up to 1, indicating the presence of multiphoton components. The reason for this behavior is still under investigation and goes beyond the scope of this paper.

If not stated otherwise, for the following measurements we fix $g^{(2)}(0) \approx 0.23$ and $p_{\text{gen}} \approx 12\%$. The emitted photon has a steep leading edge followed by a slower exponential decay, with a full width at half maximum (FWHM) of the entire photon of approximately 120 ns (see Fig. 3 at time zero).

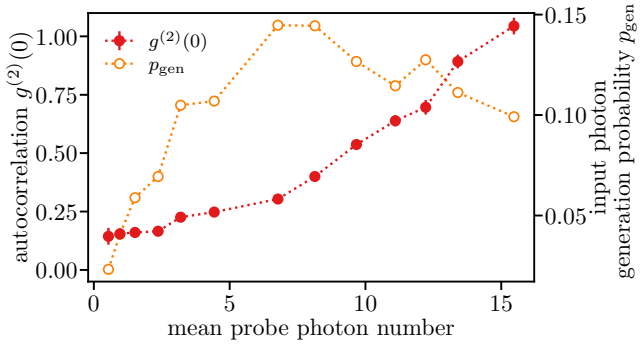

FIG. 2. The dependence of $g^{(2)}(0)$ and p_{gen} on the mean probe photon number. p_{gen} follows the Rabi cycle, decreasing for the largest values of the probe power, while $g^{(2)}(0)$ grows monotonically up to 1.

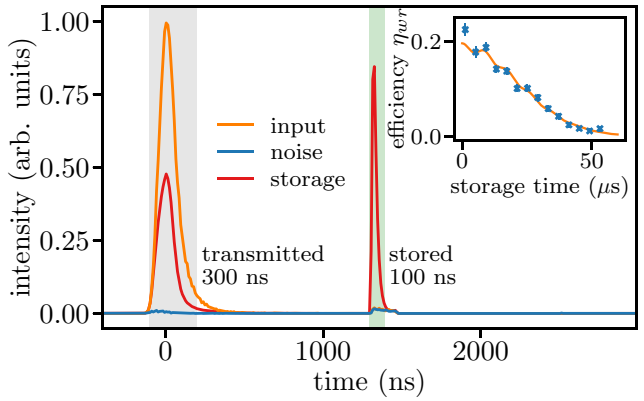

FIG. 3. The photon histogram observed at the SNSPDs after the memory. The orange histogram is the input photon alone, with no storage attempt. The red histogram presents a storage attempt. The blue histogram shows the noise without an input photon but with the atoms in the memory. The gray-shaded area is the detection window for the input and transmitted photons and the green-shaded area is the detection window for the stored photon (both windows include more than 95% of the respective wave forms). The inset shows the storage-and-retrieval efficiency as a function of the storage time with the corresponding Gaussian fit e^{-t^2/τ^2}, where τ is the memory lifetime. The fit also includes an oscillatory term accounting for spin-wave interference coming from residual population in $|5S_{1/2}, F = 2, m_F = 1\rangle$ (as an effect of imperfect Zeeman optical pumping) [51].

B. Photon storage

In this section, we demonstrate that the memory can efficiently store the generated single photon. It also offers tunability in the storage-and-retrieval process.

To characterize the memory performance, we first measure the temporal histogram of photon counts in three different situations, as shown in Fig. 3. We first detect the input single photon (orange histogram) when no storage attempt is performed, i.e., with no atoms in the memory but with control pulses. Then, a storage attempt is performed (red histogram) and we can see two peaks—the transmitted pulse, which is the part of the single input photon that is not absorbed in the storage attempt (counts in the 300 ns gray-shaded window), and the stored pulse, which is the excitation retrieved from a successful storage attempt (counts in the 100-ns green-shaded window). Finally, we measure the noise (blue histogram) by blocking the input photon while keeping all the control pulses on and the atomic cloud present. This last measurement should contain all the information about the noise present in the experiment; in particular, the noise introduced by the control pulses. We measure a corrected noise probability per trial at the output of the quantum memory, within the storage window, of $p_{\text{noise}} = 2.3(3) \times 10^{-4}$, which is derived from the detected noise probability as $p_{\text{noise}} = p^{\text{det}}_{\text{noise}}/\beta$, where $\beta = 0.34$ is the combined transmission-and-detection efficiency after the memory (at the photon frequency). This value is among the lowest reported in ground-state spin-wave memories and is comparable to other quantum memories based on cold atoms or BECs [16,35,52–54]. We attribute this noise to the control-pulse light leaking through the filter and scattering resulting from residual population on the storage transition. Four-wave mixing (4WM), which is an important source of noise in hot-vapor memories, is not observed experimentally: the noise floor remains constant as a function of the storage time, which would not be the case if 4WM introduced additional spin waves. The control beam does not couple the atomic ground state $|g_m\rangle$ to any excited state, a necessary requirement for 4WM to occur. Furthermore, the angle of 3° between the control mode and the photon mode is prohibitively large for the phase-matching condition to be satisfied [54]. 4WM does not occur in the photon source because of the ladder scheme.

The input and noise histograms serve as a reference to calculate the storage-and-retrieval efficiency $\eta_{wr} = p_s/p_{\text{in}}$, where p_s and p_{in} are the background-subtracted probabilities of detecting a stored photon (within the 100-ns detection window) and an input photon (within the 300-ns detection window), respectively. We also calculate the write-in efficiency, defined as $\eta_w = (p_{\text{in}} - p_t)/p_{\text{in}}$, where p_t is the background-subtracted detection probability of a transmitted photon (within the 300-ns detection window). From these two quantities, we infer the readout efficiency $\eta_r = \eta_{wr}/\eta_w$. We obtain a maximum storage-and-retrieval efficiency $\eta_{wr} \approx 21\%$ at a storage time of 1.2 μs. For longer storage times, the motional decoherence and the decoherence due to the stray magnetic field gradients limits the efficiency with a characteristic $1/e$ decay time of 30 μs (see the inset in Fig. 3).

For the measurement shown in Fig. 3, the SNR of the retrieved photon is 24(4). For different input numbers of photons, we measure a SNR of up to 26 (see Appendix A). An interesting figure of merit is the μ_1 parameter, defined as $\mu_1 = p_{\text{noise}}/\eta_{wr}$, which expresses the input number of photons required to have SNR = 1 at the output. In our case, we find $\mu_1 = 1.00(7) \times 10^{-3}$ (see Appendix A), which is more than 2 orders of magnitude lower than similar ground-state quantum memories based on warm atomic vapors [55–57], more than one order of magnitude lower than solid-state QMs based on rare-earth-doped solids [34,58], and similar to other quantum memories based on cold atoms [16,35,52–54].

A crucial requirement for a quantum memory is that it preserves the statistical properties of the stored photons. To show that our memory fulfills this criterion, we first adjust the mean probe photon number of the source to low values, resulting in a photon-generation probability of $p_{\text{gen}} \approx 3.0(3)\%$ (see Fig. 2). With this setting, we expect the emitted photons to be strongly nonclassical. To reduce the effect of experimental fluctuations, we collect data for 63 h. We measure $g^{(2)}(0)$ of the input ($g^{(2)}(0) = 0.20(2)$), transmitted (($g^{(2)}(0) = 0.22(3)$) and

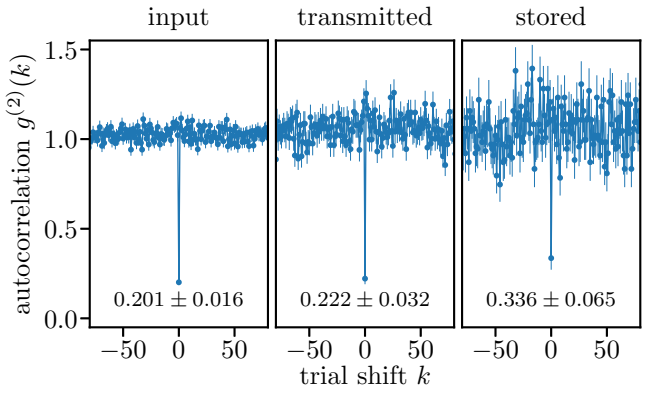

FIG. 4. The autocorrelation $g^{(2)}$ as a function of the shift between trials k for the input, transmitted, and stored photons. For trials separated by a shift $k \geq 1$, the clicks are uncorrelated, yielding $g^{(2)}(k) = 1$. Coincidences clicks in the same trial, $k = 0$, are much less frequent, suggesting photon antibunching.

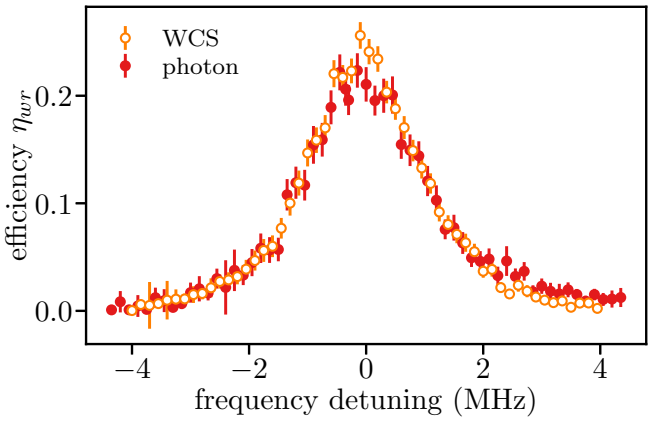

FIG. 5. The storage-and-retrieval efficiency versus the frequency detuning of the control write-in pulse for the single-photon input (red) and a WCS (orange). The frequency detuning is measured from the two-photon resonance of the input photon and the write-in control beam.

stored photons ($g^{(2)}(0) = 0.34(7)$) and obtain values well below 0.5 (see Fig. 4). This shows that the memory preserves the single-photon nature of the input photon. One can see, however, that $g^{(2)}(0)$ of the stored photon is significantly larger than the $g^{(2)}(0)$ of the input photon. We expect that the main source of degradation of $g^{(2)}(0)$ is the uncorrelated noise introduced by the memory control pulses. We develop a simple model, discussed in Appendix D, to quantify the effect of uncorrelated noise on $g^{(2)}(0)$. The model predicts $g_m^{(2)}(0) = 0.33(4)$ for a stored photon, taking into account a measured SNR of 11(2) and the measured input $g^{(2)}(0)$. For this data set, the model is in agreement with the measured data, within the error bars. We also perform several other measurements (see Appendix D, with integration times of around 10–16 h per data point) for different values of input $g^{(2)}(0)$. While the model reproduces the trend qualitatively, there is a large point-to-point fluctuation that we attribute to low statistics and experimental fluctuations.

Our memory offers significant tunability in the write-in process that may prove useful in future hybrid quantum networks [59]. We start by showing that the memory can adapt to the input-photon frequency. For that, we set the input-photon detuning to $\delta = -52$ MHz and we vary the frequency of the control-beam pulse. The maximum efficiency is observed for the two-photon resonance (see Fig. 5), achieving optimum storage conditions for the input photon.

The width of the curve depends on the spectral properties of the input photon. Bandwidth-limited photons (i.e., photons that exhibit the minimum bandwidth for a given temporal duration) are desirable because with them one can achieve a high Hong-Ou-Mandel interference visibility over the whole duration of the pulse [60,61]. Use of the whole duration of the pulse would result in higher entanglement-distribution rates. Therefore, in order to benchmark the spectral properties of the input photon, we repeat the measurement with a weak coherent state (WCS) with the same wave shape, center frequency, and mean number of photons. This WCS is derived from a laser exhibiting a line width much smaller than the bandwidth of the pulse. As can be seen in Fig. 5, the two spectra overlap very well, suggesting that the input photon is close to bandwidth limited.

Using classical light pulses, we also perform storage at detunings $\delta = -32$ MHz and $\delta = -72$ MHz (not shown here). For these values, no significant change of storage and retrieval efficiency is observed, suggesting that the input-photon detuning can be varied within this range. Eventually, the detuning will be limited by the proximity to other atomic levels.

We also study the bandwidth of our memory by sending WCSs of different durations (with FWHMs of $8 - 800$ ns). We show the results in Appendix B, suggesting that the memory can accommodate pulses of very different lengths without changing its efficiency.

Another interesting feature of the memory is that one can control how much of the input photon is absorbed and how much is transmitted. By varying the write-in control-beam power, one can change η_w as shown in Fig. 6 (top). This effectively changes the splitting ratio p_s/p_t between the stored and the transmitted photon pulse. Our memory can therefore be used as a temporal beam splitter [62] with a tunable splitting ratio, which may have applications in the quantum repeater architecture mentioned in Sec. I [33]. Substituting the BS + QM with only the QM and guiding the transmitted light directly to the intermediate station relaxes the requirements for the storage efficiencies to approach unity. To investigate this possibility, we plot p_s/p_t (see Fig. 6, bottom). It peaks for intermediate

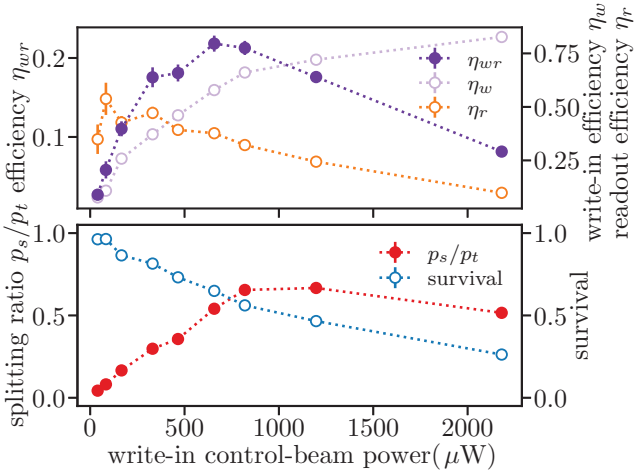

FIG. 6. The storage efficiencies, survival probability, and splitting ratio as a function of the write-in control-beam power.

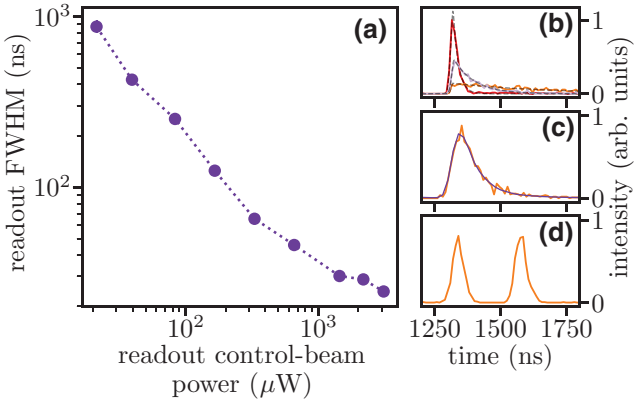

FIG. 7. The stored-photon wave-shape tunability. (a) The dependence of the stored-photon duration on the readout control-beam power. (b) Selected wave shapes of the stored photons from (a) and their corresponding fits. (c) The stored-photon wave shape (solid orange) exactly matching the input-photon wave shape (dashed blue). (d) A stored photon shaped as a time-bin qubit.

values of the write-in control-beam powers and decays for higher values. This stands in contrast to the monotonically growing η_w and is a result of η_r decreasing with the control power. We attribute this behavior of η_r to the asymmetrical distribution of the spin wave in the ensemble, when large write-in control powers are used [50,63]. With an increasing write power, the spin wave starts to have a more asymmetric shape, being mostly created at the beginning of the ensemble. This effect is known to limit the retrieval efficiency, especially in the forward-retrieval configuration [64–66].

In Fig. 6 (bottom), we also plot the survival efficiency $(p_s + p_t)/p_{\text{in}}$, the normalized probability of detecting a transmitted or stored photon per trial. We observe that it decreases with an increasing control power due to the decrease of the readout efficiency. With current conditions, the tunability range of p_s/p_t is limited but we expect that backward retrieval should considerably improve the readout efficiency at high write power, which will increase the survival probability [63]. As a first application of the single-photon temporal beam splitter, we use the two temporal output modes of the memory to measure the antibunching parameter. For the measurement presented in Fig. 4, we obtain a $g^{(2)}(0) = 0.28(2)$ with a significantly increased count rate with respect to the case where we split each output mode with a standard BS.

Our memory also offers shape tunability of the stored photons [67]. In particular, one can retrieve photons with very different lengths (with a FWHM of 25–900 ns) by changing the readout control-beam power [see Figs. 7(a) and 7(b)]. We read out the memory with a square-shaped pulse, resulting in a steep leading edge of the retrieved photon and a more slowly decaying trailing edge. We fit the former with a Gaussian function and the latter with an exponential and obtain the total FWHM of the photon. One can also use more complex wave forms for the readout control pulse to shape the readout photon, e.g., reproducing the input photon or a time-bin qubit [see Figs. 7(c) and 7(d)]. This capability would allow for matching differently shaped photons emitted by different sources. We do not observe significant reduction of η_{wr} for different readout-pulse shapes, in agreement with the theory [68].

IV. CONCLUSIONS

We demonstrate the storage and retrieval of an on-demand single photon generated in one Rydberg-based atomic ensemble in another cold atomic ensemble through a Raman memory protocol. We achieve a 21% memory efficiency and a SNR of up to 26 for the retrieved photon, leading to a μ_1 of $1.00(7) \times 10^{-3}$. This allows us to observe only a moderate degradation of the single-photon statistics. We show the adaptability of our memory in frequency and bandwidth. Moreover, we evaluate the performance of the built-in temporal beam splitter offered by the Raman memory. Lastly, we show that we can shape the temporal wave form of the retrieved photon by shaping the readout-pulse power and wave form. These results are a step forward in the implementation of efficient quantum repeater links using single-photon sources. In that context, one interesting advantage of having the source and the memory residing in different ensembles is that they can be optimized independently. This allows for efficient single-photon generation and storage and facilitates the use of multiplexed quantum memories [17,30], which would significantly improve repeater entanglement-generation rates.

Several improvements should be applied to our experiment before it can become a practical alternative. The generation efficiency of the single photon from the Rydberg ensemble could be increased by increasing the OD

of the ensemble and/or by embedding the ensemble in a low-finesse cavity [69]. The quality of the single photon (as measured by the autocorrelation function $g^{(2)}(0)$) could also be improved by addressing a slightly smaller ensemble and by reaching a higher principal quantum number level to increase the Rydberg blockade radius, as has been shown in Ref. [47], where $g^{(2)}(0)$ values smaller than 10^{-3} have been measured. Regarding the Raman quantum memory, higher storage-and-retrieval efficiencies could also be reached by increasing the OD of the ensemble [16] and using backward retrieval [65], or with an impedance-matched cavity. Backward retrieval will also improve the survival probability and the performance of the temporal beam splitter. Finally, a longer storage time of up to 1 s could be achieved by using magnetically insensitive transitions and by loading the ensemble into an optical lattice to suppress motion-induced dephasing [70].

ACKNOWLEDGMENTS

We acknowledge interesting discussions with Gerhard Rempe. L.H. and J.L. acknowledge funding from the European Union Horizon 2020 research and innovation program under the Marie Skłodowska-Curie Grant Agreement No. 713729. This project received funding from the Government of Spain (PID2019-106850RB-I00 project and Severo Ochoa CEX2019-000910-S), funded by MCIN/AEI/10.13039/501100011033, from MCIN with funding from European Union NextGenerationEU (PRTR-C17.I1), from the European Union Horizon 2020 research and innovation program under Grant Agreement No. 899275 (DAALI), from the Gordon and Betty Moore Foundation through Grant No. GBMF7446 to H.d.R., from Fundació Cellex, from Fundació Mir-Puig, and from Generalitat de Catalunya (CERCA, AGAUR).

L.H. and J.L. contributed equally to this work.

Note added.—While finalizing our experiment, we learned about a recent experiment where a single photon generated by Rydberg atoms was stored in an atomic ensemble using electromagnetically induced transparency [71].

APPENDIX A: ESTIMATION OF μ_1 PARAMETER (WITH SINGLE-PHOTON INPUT)

An important figure of merit for a quantum memory is the parameter μ_1, which is defined as the minimum mean number of input photons to have a SNR of 1 for the stored photon.

In Fig. 8, we show a measurement of the SNR in the readout (stored) detection window by varying the mean number of single photons at the input of the Raman memory. This is achieved by varying the Rydberg probe power (see Fig. 2). From a linear fit that passes through zero, we estimate a μ_1 parameter of $1.00(7) \times 10^{-3}$.

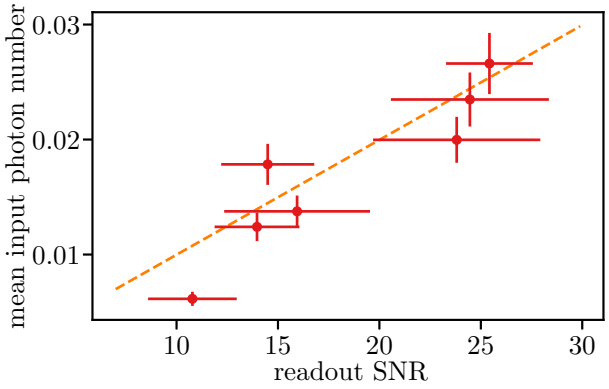

FIG. 8. The mean number of single photons at the input of the memory as a function of the readout SNR. The orange dashed line is a linear fit that passes through zero. The slope of this line corresponds to μ_1.

APPENDIX B: ACCEPTANCE-MEMORY BANDWIDTH (WITH WEAK COHERENT STATES)

To understand whether the memory efficiency is limited by its acceptance bandwidth, we measure the storage-and-retrieval efficiency for input pulses with variable duration. The maximum duration of the single photons generated at the source is limited by the dephasing rate of the collective Rydberg excitations. Moreover, the minimum duration is limited by the coupling beam power, leading to a FWHM greater than approximately 90 ns. Therefore, we instead send WCS pulses with mean number of photons well below 1. The duration of the WCS pulses is controlled

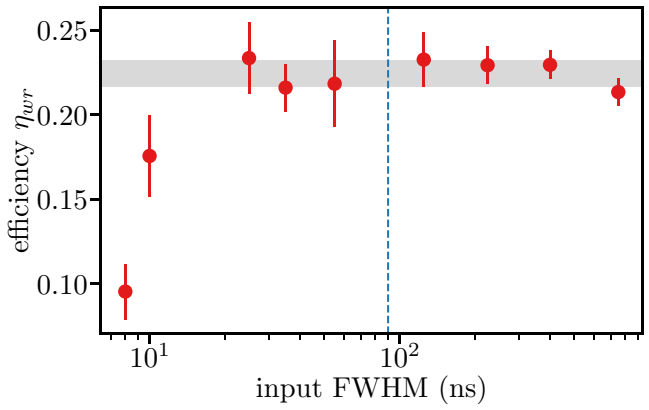

FIG. 9. The storage-and-retrieval efficiency η_{wr} as a function of the temporal duration (FWHM) of WCS input pulses with a Gaussian shape. The gray horizontally shaded area represents the mean (0.225) and standard deviation (0.008) of the efficiency for input pulse durations above 25 ns. The blue dashed vertical line represents the minimum duration of the single photon generated by the Rydberg-based source (approximately 90 ns FWHM). For each data point, the write-in control-pulse power, shape, and delay are optimized.

by an AOM, achieving pulses as short as 8 ns (FWHM). We send Gaussian-shaped pulses because the conversion to bandwidth is straightforward.

The results are shown in Fig. 9. For pulse durations between 25 ns and 750 ns, the storage-and-retrieval efficiency η_{wr} remains constant and is in agreement with the efficiencies measured for the single-photon input. It is only for pulse durations below 25 ns, corresponding to a bandwidth of approximately 17.6 MHz (assuming transform-limited Gaussian pulses), that the storage-and-retrieval efficiency drops. We attribute this drop to limited control power and a finite AOM rise time, resulting in a smaller pulse area. For input pulses much longer than 750 ns (not characterized here), the efficiency is expected to be eventually limited by the lifetime of the memory [67]. We estimate the bandwidth of the single photon to be approximately 4 MHz, assuming bandwidth-limited Gaussian pulses.

APPENDIX C: MEMORY PERFORMANCE WITH OPTICAL DEPTH (WITH WEAK COHERENT STATES)

It is instructive to analyze the memory performance when varying the OD, since the OD governs how efficiently the incoming light pulse is absorbed and reemitted. For that, we vary the trapping laser power during the magneto-optical trap stage and use the shortest interrogation time possible to be able to scan the full range of ODs available.

The OD value is obtained by measuring the transmission of a continuous coherent beam around resonance with the $|g_s\rangle \rightarrow |e_s\rangle$ transition. The results are shown in Fig. 10. The storage efficiencies are measured for WCS pulses as input, shaped to mimic the temporal profile of the single photons generated in the Rydberg-based source.

We observe a saturation of the storage-and-retrieval efficiency $\eta_{wr} = \eta_w \cdot \eta_r$ for an OD around 6.5. However, the write-in efficiency η_w still seems to profit from a higher OD, while the readout efficiency η_r is already at the maximum. One possible explanation for this behavior is reemission followed by reabsorption, which limits the maximal retrieval efficiency in forward retrieval (i.e., when the photon field is retrieved from the medium copropagating to the input) [72,73].

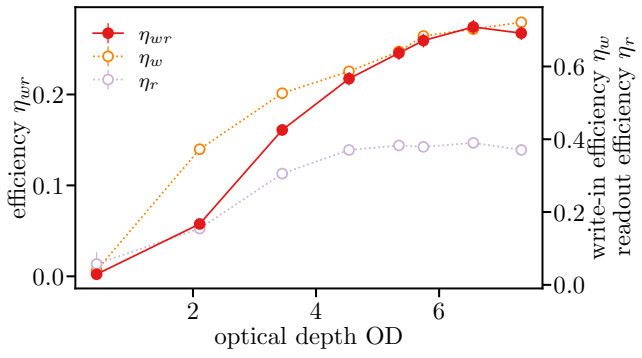

FIG. 10. The storage efficiencies η_w, η_r, and η_{wr} as a function of the OD of the ensemble for weak coherent input pulses with a mean photon number of 0.077. For each data point, the write-in control-pulse power and the delay are optimized.

Data in the main text are taken for an OD around 5, which constitutes a compromise between achieving a high η_{wr} while at the same time maintaining an acceptable duty cycle for data acquisition.

APPENDIX D: EFFECT OF THE NOISE IN THE MEASURED AUTOCORRELATION FUNCTION OF SINGLE PHOTONS

Noise originating either from the control beam or its interaction with the ensemble can lead to uncorrelated coincidences that affect the measured single-photon statistics of the transmitted or stored photons. In the absence of a control field and atoms, the unperturbed autocorrelation is measured as

$$g^{(2)}_{\text{in}}(0) = \frac{c_{1,2}}{p_1 p_2}, \tag{D1}$$

where p_1 (p_2) is the probability of detection per trial on detector 1 (2) and $c_{1,2}$ is the probability of coincidence detection per trial between both detectors. When a storage attempt is performed, the noise introduced by the control pulses and the atoms alter the probabilities for detection and coincidences as follows:

$$\tilde{c}_{1,2} = c_{1,2} + p_1 p_{n,2} + p_2 p_{n,1} + p_{n,1} p_{n,2}, \tag{D2}$$

$$\tilde{p}_{1\,(2)} = p_{1\,(2)} + p_{n,1\,(2)}. \tag{D3}$$

Here, $p_{n,1}$ ($p_{n,2}$) is the noise probability for detector 1 (2). The autocorrelation is therefore

$$g^{(2)}_{\text{out}}(0) = \frac{\tilde{c}_{1,2}}{\tilde{p}_1 \tilde{p}_2} = \frac{p_{12} + p_1 p_{n,2} + p_2 p_{n,1} + p_{n,1} p_{n,2}}{p_1 p_2 + p_{n,1} p_2 + p_{n,2} p_1 + p_{n,1} p_{n,2}}, \tag{D4}$$

which can be rewritten in terms of SNRs as

$$g^{(2)}_{\text{out}}(0) = \frac{g^{(2)}_{\text{in}}(0) + 1/s_1 + 1/s_2 + 1/(s_1 s_2)}{1 + 1/s_1 + 1/s_2 + 1/(s_1 s_2)}, \tag{D5}$$

where $s_{1\,(2)} = p_{1\,(2)}/p_{n,1\,(2)}$ is the signal-to-noise ratio for detector 1 (2).

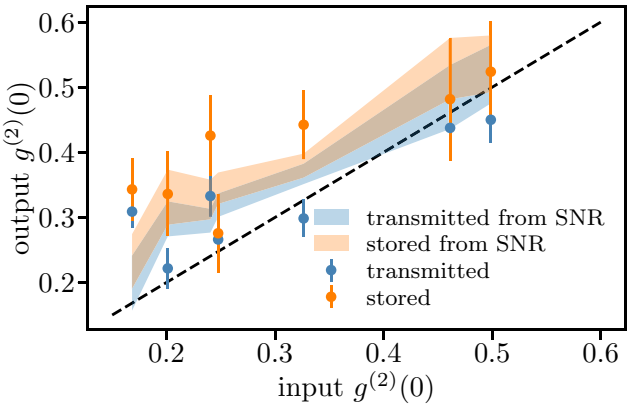

FIG. 11. The output $g^{(2)}(0)$ of the transmitted and stored photons as a function of the input $g^{(2)}(0)$. The dashed black line shows the autocorrelation after the memory equals the input. The shaded areas show the autocorrelation for the transmitted and stored photons as expected from Eq. (D6), taking into account the uncertainty in $g^{(2)}_{\text{in}}(0)$ and the SNR.

Assuming that the SNR is the same for both detectors, this expression finally simplifies to

$$g^{(2)}_{\text{out}}(0) = \frac{g^{(2)}_{\text{in}}(0) + 2/s + 1/s^2}{1 + 2/s + 1/s^2}. \tag{D6}$$

In Fig. 11, we characterize the effect of noise on the $g^{(2)}(0)$ of the stored and the transmitted photons for different values of $g^{(2)}(0)$ of the input photon (i.e., with no storage attempt). The input $g^{(2)}(0)$ is scanned by varying the mean number of photons in the probe (see Fig. 2 in the main text). We can see that, in general, the output $g^{(2)}(0)$ degrades compared to the input $g^{(2)}(0)$ and that the autocorrelation of the transmitted photon is better than that of the stored photon. Therefore, we can conclude that the model qualitatively reproduces the expected trend. We attribute the imperfection in the quantitative analysis to low statistics and experimental fluctuations.

[1] H. J. Kimble, The quantum Internet, Nature **453**, 1023 (2008).

[2] H.-J. Briegel, W. Dür, J. I. Cirac, and P. Zoller, Quantum Repeaters: The Role of Imperfect Local Operations in Quantum Communication, Phys. Rev. Lett. **81**, 5932 (1998).

[3] L.-M. Duan, M. D. Lukin, J. I. Cirac, and P. Zoller, Long-distance quantum communication with atomic ensembles and linear optics, Nature **414**, 413 (2001).

[4] N. Sangouard, C. Simon, H. de Riedmatten, and N. Gisin, Quantum repeaters based on atomic ensembles and linear optics, Rev. Mod. Phys. **83**, 33 (2011).

[5] S. Ritter, C. Nölleke, C. Hahn, A. Reiserer, A. Neuzner, M. Uphoff, M. Mücke, E. Figueroa, J. Bochmann, and G. Rempe, An elementary quantum network of single atoms in optical cavities, Nature **484**, 195 (2012).

[6] S. Langenfeld, P. Thomas, O. Morin, and G. Rempe, Quantum Repeater Node Demonstrating Unconditionally Secure Key Distribution, Phys. Rev. Lett. **126**, 230506 (2021).

[7] A. Stute, B. Casabone, P. Schindler, T. Monz, P. O. Schmidt, B. Brandstätter, T. E. Northup, and R. Blatt, Tunable ion-photon entanglement in an optical cavity, Nature **485**, 482 (2012).

[8] D. Hucul, I. V. Inlek, G. Vittorini, C. Crocker, S. Debnath, S. M. Clark, and C. Monroe, Modular entanglement of atomic qubits using photons and phonons, Nat. Phys. **11**, 37 (2015).

[9] V. Krutyanskiy, M. Meraner, J. Schupp, V. Krcmarsky, H. Hainzer, and B. P. Lanyon, Light-matter entanglement over 50 km of optical fibre, npj Quantum Inf. **5**, 72 (2019).

[10] L. J. Stephenson, D. P. Nadlinger, B. C. Nichol, S. An, P. Drmota, T. G. Ballance, K. Thirumalai, J. F. Goodwin, D. M. Lucas, and C. J. Ballance, High-Rate, High-Fidelity Entanglement of Qubits across an Elementary Quantum Network, Phys. Rev. Lett. **124**, 110501 (2020).

[11] T. Chanelière, D. N. Matsukevich, S. D. Jenkins, S.-Y. Lan, T. A. B. Kennedy, and A. Kuzmich, Storage and retrieval of single photons transmitted between remote quantum memories, Nature **438**, 833 (2005).

[12] C. W. Chou, H. de Riedmatten, D. Felinto, S. V. Polyakov, S. J. van Enk, and H. J. Kimble, Measurement-induced entanglement for excitation stored in remote atomic ensembles, Nature **438**, 828 (2005).

[13] C.-W. Chou, J. Laurat, H. Deng, K. S. Choi, H. de Riedmatten, D. Felinto, and H. J. Kimble, Functional quantum nodes for entanglement distribution over scalable quantum networks., Science (New York) **316**, 1316 (2007).

[14] Z.-S. Yuan, Y.-A. Chen, B. Zhao, S. Chen, J. Schmiedmayer, and J.-W. Pan, Experimental demonstration of a BDCZ quantum repeater node, Nature **454**, 1098 (2008).

[15] D. N. Matsukevich, T. Chaneliere, S. D. Jenkins, S.-Y. Lan, T. A. B. Kennedy, and A. Kuzmich, Entanglement of Remote Atomic Qubits, Phys. Rev. Lett. **96**, 030405 (2006).

[16] M. Cao, F. Hoffet, S. Qiu, A. S. Sheremet, and J. Laurat, Efficient reversible entanglement transfer between light and quantum memories, Optica **7**, 1440 (2020).

[17] L. Heller, P. Farrera, G. Heinze, and H. de Riedmatten, Cold-Atom Temporally Multiplexed Quantum Memory with Cavity-Enhanced Noise Suppression, Phys. Rev. Lett. **124**, 210504 (2020).

[18] Y. Yu, F. Ma, X.-Y. Luo, B. Jing, P.-F. Sun, R.-Z. Fang, C.-W. Yang, H. Liu, M.-Y. Zheng, X.-P. Xie, W.-J. Zhang, L.-X. You, Z. Wang, T.-Y. Chen, Q. Zhang, X.-H. Bao, and J.-W. Pan, Entanglement of two quantum memories via fibres over dozens of kilometres, Nature **578**, 240 (2020).

[19] P. C. Humphreys, N. Kalb, J. P. J. Morits, R. N. Schouten, R. F. L. Vermeulen, D. J. Twitchen, M. Markham, and R. Hanson, Deterministic delivery of remote entanglement on a quantum network, Nature **558**, 268 (2018).

[20] M. K. Bhaskar, R. Riedinger, B. Machielse, D. S. Levonian, C. T. Nguyen, E. N. Knall, H. Park, D. Englund, M. Lončar, D. D. Sukachev, and M. D. Lukin, Experimental demonstration of memory-enhanced quantum communication, Nature **580**, 60 (2020).

[21] H. de Riedmatten, M. Afzelius, M. U. Staudt, C. Simon, and N. Gisin, A solid-state light-matter interface at the single-photon level, Nature **456**, 773 (2008).
[22] M. P. Hedges, J. J. Longdell, Y. Li, and M. J. Sellars, Efficient quantum memory for light, Nature **465**, 1052 (2010).
[23] E. Saglamyurek, N. Sinclair, J. Jin, J. A. Slater, D. Oblak, F. Bussieres, M. George, R. Ricken, W. Sohler, and W. Tittel, Broadband waveguide quantum memory for entangled photons, Nature **469**, 512 (2011).
[24] C. Clausen, I. Usmani, F. Bussieres, N. Sangouard, M. Afzelius, H. de Riedmatten, and N. Gisin, Quantum storage of photonic entanglement in a crystal, Nature **469**, 508 (2011).
[25] D. Lago-Rivera, S. Grandi, J. V. Rakonjac, A. Seri, and H. de Riedmatten, Telecom-heralded entanglement between multimode solid-state quantum memories, Nature **594**, 37 (2021).
[26] X. Liu, J. Hu, Z.-F. Li, X. Li, P.-Y. Li, P.-J. Liang, Z.-Q. Zhou, C.-F. Li, and G.-C. Guo, Heralded entanglement distribution between two absorptive quantum memories, Nature **594**, 41 (2021).
[27] C. Simon, H. de Riedmatten, M. Afzelius, N. Sangouard, H. Zbinden, and N. Gisin, Quantum Repeaters with Photon Pair Sources and Multimode Memories, Phys. Rev. Lett. **98**, 190503 (2007).
[28] O. A. Collins, S. D. Jenkins, A. Kuzmich, and T. A. B. Kennedy, Multiplexed memory-insensitive quantum repeaters, Phys. Rev. Lett. **98**, 060502 (2007).
[29] S.-Y. Lan, A. G. Radnaev, O. A. Collins, D. N. Matsukevich, T. A. Kennedy, and A. Kuzmich, A multiplexed quantum memory, Opt. Express **17**, 13639 (2009).
[30] Y. Pu, N. Jiang, W. Chang, H. Yang, C. Li, and L. Duan, Experimental realization of a multiplexed quantum memory with 225 individually accessible memory cells, Nat. Commun. **8**, 15359 (2017).
[31] W. Chang, C. Li, Y.-K. Wu, N. Jiang, S. Zhang, Y.-F. Pu, X.-Y. Chang, and L.-M. Duan, Long-distance entanglement between a multiplexed quantum memory and a telecom photon, Phys. Rev. X **9**, 041033 (2019).
[32] D. Felinto, C. W. Chou, J. Laurat, E. W. Schomburg, H. de Riedmatten, and H. J. Kimble, Conditional control of the quantum states of remote atomic memories for quantum networking, Nat. Phys. **2**, 844 (2006).
[33] N. Sangouard, C. Simon, J. Minar, H. Zbinden, H. de Riedmatten, and N. Gisin, Long-distance entanglement distribution with single-photon sources, Phys. Rev. A **76**, 050301 (R) (2007).
[34] A. Seri, A. Lenhard, D. Rieländer, M. Gündoğan, P. M. Ledingham, M. Mazzera, and H. de Riedmatten, Quantum correlations between single telecom photons and a multimode on-demand solid-state quantum memory, Phys. Rev. X **7**, 021028 (2017).
[35] D. S. Ding, W. Zhang, Z. Y. Zhou, S. Shi, B. S. Shi, and G. C. Guo, Raman quantum memory of photonic polarized entanglement, Nat. Photonics **9**, 332 (2015).
[36] Y. Wang, J. Li, S. Zhang, K. Su, Y. Zhou, K. Liao, S. Du, H. Yan, and S.-L. Zhu, Efficient quantum memory for single-photon polarization qubits, Nat. Photonics **13**, 346 (2019).
[37] N. Akopian, L. Wang, A. Rastelli, O. G. Schmidt, and V. Zwiller, Hybrid semiconductor-atomic interface: Slowing down single photons from a quantum dot, Nat. Photonics **5**, 230 (2011).
[38] P. Siyushev, G. Stein, J. Wrachtrup, and I. Gerhardt, Molecular photons interfaced with alkali atoms, Nature **509**, 66 (2014).
[39] J.-S. Tang, Z.-Q. Zhou, Y.-T. Wang, Y.-L. Li, X. Liu, Y.-L. Hua, Y. Zou, S. Wang, D.-Y. He, G. Chen, Y.-N. Sun, Y. Yu, M.-F. Li, G.-W. Zha, H.-Q. Ni, Z.-C. Niu, C.-F. Li, and G.-C. Guo, Storage of multiple single-photon pulses emitted from a quantum dot in a solid-state quantum memory, Nat. Commun. **6**, 8652 (2015).
[40] T. Kroh, J. Wolters, A. Ahlrichs, A. W. Schell, A. Thoma, S. Reitzenstein, J. S. Wildmann, E. Zallo, R. Trotta, A. Rastelli, O. G. Schmidt, and O. Benson, Slow and fast single photons from a quantum dot interacting with the excited state hyperfine structure of the cesium D1-line, Sci. Rep. **9**, 13728 (2019).
[41] M. Lettner, M. Mücke, S. Riedl, C. Vo, C. Hahn, S. Baur, J. Bochmann, S. Ritter, S. Dürr, and G. Rempe, Remote Entanglement between a Single Atom and a Bose-Einstein Condensate, Phys. Rev. Lett. **106**, 210503 (2011).
[42] Y. O. Dudin and A. Kuzmich, Strongly interacting Rydberg excitations of a cold atomic gas, Science (New York) **336**, 887 (2012).
[43] D. Maxwell, D. J. Szwer, D. Paredes-Barato, H. Busche, J. D. Pritchard, A. Gauguet, K. J. Weatherill, M. P. A. Jones, and C. S. Adams, Storage and Control of Optical Photons Using Rydberg Polaritons, Phys. Rev. Lett. **110**, 103001 (2013).
[44] L. Li and A. Kuzmich, Quantum memory with strong and controllable Rydberg-level interactions, Nat. Commun. **7**, 13618 (2016).
[45] J. Li, M.-T. Zhou, C.-W. Yang, P.-F. Sun, J.-L. Liu, X.-H. Bao, and J.-W. Pan, Semideterministic entanglement between a single photon and an atomic ensemble, Phys. Rev. Lett. **123**, 140504 (2019).
[46] L. Li, Y. O. Dudin, and A. Kuzmich, Entanglement between light and an optical atomic excitation, Nature **498**, 466 (2013).
[47] D. P. Ornelas-Huerta, A. N. Craddock, E. A. Goldschmidt, A. J. Hachtel, Y. Wang, P. Bienias, A. V. Gorshkov, S. L. Rolston, and J. V. Porto, On-demand indistinguishable single photons from an efficient and pure source based on a Rydberg ensemble, Optica **7**, 813 (2020).
[48] A. Padrón-Brito, J. Lowinski, P. Farrera, K. Theophilo, and H. de Riedmatten, Probing the indistinguishability of single photons generated by Rydberg atomic ensembles, Phys. Rev. Res. **3**, 033287 (2021).
[49] M. D. Lukin, M. Fleischhauer, R. Cote, L. M. Duan, D. Jaksch, J. I. Cirac, and P. Zoller, Dipole Blockade and Quantum Information Processing in Mesoscopic Atomic Ensembles, Phys. Rev. Lett. **87**, 037901 (2001).
[50] J. Nunn, I. A. Walmsley, M. G. Raymer, K. Surmacz, F. C. Waldermann, Z. Wang, and D. Jaksch, Mapping broadband single-photon wave packets into an atomic memory, Phys. Rev. A **75**, 011401 (2007).
[51] B. Albrecht, P. Farrera, G. Heinze, M. Cristiani, and H. de Riedmatten, Controlled Rephasing of Single Collective

Spin Excitations in a Cold Atomic Quantum Memory, Phys. Rev. Lett. **115**, 160501 (2015).

[52] E. Saglamyurek, T. Hrushevskyi, L. Cooke, A. Rastogi, and L. J. LeBlanc, Single-photon-level light storage in cold atoms using the Autler-Townes splitting protocol, Phys. Rev. Res. **1**, 022004 (2019).

[53] M. Lettner, Ein Bose-Einstein-Kondensat Als Quantenspeicher Für Zwei-Teilchen-Verschränkung, Ph.D. thesis, Fakultät für Physik, Technische Universität München, München (2011).

[54] E. Saglamyurek, T. Hrushevskyi, A. Rastogi, L. W. Cooke, B. D. Smith, and L. J. LeBlanc, Storing short single-photon-level optical pulses in Bose-Einstein condensates for high-performance quantum memory, New J. Phys. **23**, 043028 (2021).

[55] J. Wolters, G. Buser, A. Horsley, L. Béguin, A. Jöckel, J.-P. Jahn, R. J. Warburton, and P. Treutlein, Simple Atomic Quantum Memory Suitable for Semiconductor Quantum Dot Single Photons, Phys. Rev. Lett. **119**, 060502 (2017).

[56] S. E. Thomas, T. M. Hird, J. H. D. Munns, B. Brecht, D. J. Saunders, J. Nunn, I. A. Walmsley, and P. M. Ledingham, Raman quantum memory with built-in suppression of four-wave-mixing noise, Phys. Rev. A **100**, 033801 (2019).

[57] M. Namazi, C. Kupchak, B. Jordaan, R. Shahrokhshahi, and E. Figueroa, Ultralow-Noise Room-Temperature Quantum Memory for Polarization Qubits, Phys. Rev. Appl. **8**, 034023 (2017).

[58] M. Gündoğan, P. M. Ledingham, K. Kutluer, M. Mazzera, and H. de Riedmatten, Solid State Spin-Wave Quantum Memory for Time-Bin Qubits, Phys. Rev. Lett. **114**, 230501 (2015).

[59] N. Maring, P. Farrera, K. Kutluer, M. Mazzera, G. Heinze, and H. De Riedmatten, Photonic quantum state transfer between a cold atomic gas and a crystal, Nature **551**, 485 (2017).

[60] C. K. Hong, Z. Y. Ou, and L. Mandel, Measurement of Subpicosecond Time Intervals between Two Photons by Interference, Phys. Rev. Lett. **59**, 2044 (1987).

[61] T. Legero, T. Wilk, A. Kuhn, and G. Rempe, Time-resolved two-photon quantum interference, Appl. Phys. B **77**, 797 (2003).

[62] K. F. Reim, J. Nunn, X.-M. Jin, P. S. Michelberger, T. F. M. Champion, D. G. England, K. C. Lee, W. S. Kolthammer, N. K. Langford, and I. A. Walmsley, Multipulse Addressing of a Raman Quantum Memory: Configurable Beam Splitting and Efficient Readout, Phys. Rev. Lett. **108**, 263602 (2012).

[63] A. V. Gorshkov, A. Andre, M. D. Lukin, and A. S. Sørensen, Photon storage in Lambda-type optically dense atomic media. II. Free-space model, Phys. Rev. A **76**, 033805 (2007).

[64] A. S. Sheremet, L. V. Gerasimov, I. M. Sokolov, D. V. Kupriyanov, O. S. Mishina, E. Giacobino, and J. Laurat, Quantum memory for light via a stimulated off-resonant Raman process: Beyond the three-level Λ-scheme approximation, Phys. Rev. A **82**, 033838 (2010).

[65] P. Vernaz-Gris, A. D. Tranter, J. L. Everett, A. C. Leung, K. V. Paul, G. T. Campbell, P. K. Lam, and B. C. Buchler, High-performance Raman memory with spatio-temporal reversal, Opt. Express **26**, 12424 (2018).

[66] Y. H. Chen, M. J. Lee, I. C. Wang, S. Du, Y. F. Chen, Y. C. Chen, and I. A. Yu, Coherent Optical Memory with High Storage Efficiency and Large Fractional Delay, Phys. Rev. Lett. **110**, 083601 (2013).

[67] P. Farrera, G. Heinze, B. Albrecht, M. Ho, M. Chávez, C. Teo, N. Sangouard, and H. de Riedmatten, Generation of single photons with highly tunable wave shape from a cold atomic ensemble, Nat. Commun. **7**, 13556 (2016).

[68] J. Nunn, Quantum memory in atomic ensembles, Ph.D. thesis, University of Oxford, St. John's College, Oxford (2008).

[69] C.-W. Yang, J. Li, M.-T. Zhou, X. Jiang, X.-H. Bao, and J.-W. Pan, Single-shot measurement of a Rydberg superatom via collective photon burst (2021), ArXiv:2106.10858.

[70] X.-J. Wang, S.-J. Yang, P.-F. Sun, B. Jing, J. Li, M.-T. Zhou, X.-H. Bao, and J.-W. Pan, Cavity-Enhanced Atom-Photon Entanglement with Subsecond Lifetime, Phys. Rev. Lett. **126**, 090501 (2021).

[71] Y. Yu, P.-F. Sun, Y.-Z. Zhang, B. Bai, Y.-Q. Fang, X.-Y. Luo, Z.-Y. An, J. Li, J. Zhang, F. Xu, X.-H. Bao, and J.-W. Pan, Measurement-Device-Independent Verification of a Quantum Memory, Phys. Rev. Lett. **127**, 160502 (2021).

[72] K. F. Reim, J. Nunn, V. O. Lorenz, B. J. Sussman, K. C. Lee, N. K. Langford, D. Jaksch, and I. A. Walmsley, Towards high-speed optical quantum memories, Nat. Photonics **4**, 218 (2010).

[73] A. V. Gorshkov, A. Andre, M. Fleischhauer, A. S. Sørensen, and M. D. Lukin, Universal Approach to Optimal Photon Storage in Atomic Media, Phys. Rev. Lett. **98**, 123601 (2007).